Application of nanofiltration model for prediction of rejecting typical refractory compounds in coal gasification brine

Kun Li[a], Wencheng Ma[a], Hongjun Han[a], Chunyan Xu[a,*], Yuxing Han[b,*], Dexin Wang[a], Weiwei Ma[a], Zhengwen Zhang[a]

[a]State Key Laboratory of Urban Water Resource and Environment, Harbin Institute of Technology, Harbin 150090, China,
Tel. +86 451 87649777; Fax: +86 451 86283082; emails: 15946091166@139.com (C.Y. Xu), amyleeal@outlook.com (K. Li),
damahit@163.com (W.C. Ma), han13946003379@163.com (H.J. Han), 114010296@qq.com (D. Wang), 501234355@qq.com (W.W. Ma),
zhengwen_zhang@126.com (Z.W. Zhang)
[b]School of Engineering, South China Agriculture University, Guangzhou 510642, China, email: yuxinghan@scau.edu.cn

ABSTRACT

Nanofiltration has been widely applied in the treatment of industrial effluents, but very few work concerns in the coal gasification brine (CGB), especially in terms of removing the typical refractory compounds (TRCs) with different signs of charge and low molecular weights from it. This study investigated the separation performance of the TRCs using three nanofiltration membranes and assessed the applicability of the DSPM&DE model (Donnan steric pore model and dielectric exclusion) in predicting the TRCs rejection ratio. The TRCs rejection ratios of NF270 were greater than 79.15%, and the discrepancies between the experimental values and model data were lower than 5%. The undecane with 156.31 Da, representing the long chain n-alkanes, was exceptionally rejected and its rejection ratio reached to 98.52% at 42.04 L m^{-2} h^{-1} by NF270. The steric hindrance effect was considered the primary mechanism for separating the uncharged TRCs in the CGB. In general, the DSPM&DE model slightly underestimated the rejection of the positively charged TRCs and predicted accurately for most of the uncharged TRCs. The accuracy of the predicted rejection ratio of the DSPM&DE model for the TRCs with low molecular weight could be improved by incorporating the partition of the TRCs at the interface of solute–membrane.

Keywords: Typical refractory compounds; Brine; Nanofiltration; Near zero liquid discharge; Coal gasification wastewater

1. Introduction

The coal gasification industry has been rapidly developed in China due to its important role in energy supply in recent years. It is noteworthy that the serious environmental problems caused by the coal gasification wastewater have raised extreme concerns. The coal gasification brine (CGB) is the concentrate of the multistage reverse osmosis of the coal gasification wastewater, which possesses considerably high concentration of salts and typical refractory compounds (TRCs) with the characteristic of microbial activity inhibition, carcinogenicity, teratogenicity and mutagenicity [1]. Nevertheless, different kinds of degradation products of organic compounds are produced after the biological and advanced treatments and the residual TRCs remain in the effluent of the coal gasification wastewater. Generally, the TRCs in the CGB mainly include a considerable number of long chain n-alkanes [2], polynuclear aromatic hydrocarbons [3], esters, heterocycles, carboxylic acids, alcohols, ketones and amides [4–6].

The TRCs of CGB are regarded extremely difficult to be effectively removed due to the following two factors: (1) the

* Corresponding authors.

concentration of TRCs in the CGB is multiple times of that of effluent of coal gasification wastewater after the multi-stage reverse osmosis treatment, and the chemical oxygen demand (COD) of the CGB can be as high as 1,200 mg L^{-1}; (2) techniques such as biological treatment, electrolysis technology and ozonation technology have a poor removal of TRCs, because the considerably high concentration of salt in the CGB inhibits the biological activity [2] and reduces the oxidation of the TRCs [7].

The integrated process of reverse osmosis, evaporation and crystallization is a common method used for treating the CGB. However, a non-recyclable mixed salt is produced during this process, which is not effectively disposed by the solid waste treatment technology. Additionally, these salts exhibit the hidden dangers of secondary environmental pollution according to the Identification Standards for Hazardous Wastes General Specifications of China [8]. Therefore, the treatment of TRCs is the prime obstacle in the near-zero liquid discharge of the coal gasification industry [9].

Nanofiltration (NF) membranes demonstrate a wide application in removing the organic compounds from pharmaceutical wastewater, dyeing wastewater and surface water since it was first prepared in the 1980's [10–12]. The NF membrane can be negatively charged because the surface layer material contains ionizable functional groups [10,13,14]. In a study conducted by Chen et al. [15], the negatively charged organic compounds were more rejected in the concentrate than the uncharged organic compounds of similar size. Generally, there are several factors that affect the removal efficiency of the NF membrane, including the size and charge of organic compounds and the membrane's pore radius and charge density. Based on the previous studies, a fundamental insight into the primacy rejection mechanism of the uncharged organic compounds involves understanding the steric hindrance effect [16]. Further, the charged organic compounds are removed by the electrostatic repulsion effect and steric hindrance effect when the molecular weight (MW) of the organic compounds is greater than the molecular weight cut-off (MWCO) [17]. Nevertheless, the removal efficiency of the TRCs from the CGB by the NF membrane is not thoroughly studied as the MW of majority of TRCs is close to the MWCO of most commercial NF membranes. Therefore, the NF membranes with different characteristics have been used to test the rejection performance of the TRCs in our previous studies. It is remarkable that the NF membrane exhibited the excellent separation performance for the CGB. The results showed that the COD rejection of the tight NF membrane attained to 78.84% while that with the loose NF membrane was just 62.11% with similar membrane flux [6]. The negative rejection of monovalent ions and a high rejection of multivalent ions were observed in this experiment [6] and prior study [14]. Moreover, the sodium chloride of the NF permeate accounts for over 85% of salt in our pervious study [6]. Hence, NF is a promising technology for treating the CGB in terms of salt recovery and the removal of TRCs. It is also an environment-friendly method as it prevents the secondary pollution hazards. Comprehensively, it is significantly necessary to investigate the removal performance of the TRCs by the NF membrane.

The major limitation of NF modeling is the requirement for model parameters, such as the average pore radius (r_p),

effective membrane thickness (δ), membrane charge density (χ). In reality, more parameters are implicitly involved in the DSPM&DE model, which may include the partitioning coefficients of the solutes between water and the solid phases and hindrance factor for the solute transport in the membrane [18]. Furthermore, the accuracy of the model depends on the quantification of the coefficients of solute partition and the hindrance factors for convection as well as diffusion. Many studies have been conducted on the pharmaceutical wastewater and groundwater to improve the accuracy of the DSPM&DE model. However, studies on the removal of the TRCs from CGB by NF membranes and applicability of the DSPM&DE model in predicting the rejection of the TRCs are rather scarce.

The separation performances of 14 TRCs with different characteristics by the NF membranes were investigated, and the applicability of the DSPM&DE model for the prediction of rejection ratios was assessed in this study. The TRCs were employed as model micropollutants based on their different physicochemical properties (e.g., hydrophobicity, molecular structure and charge). They were considered the representatives of organic compounds in the CGB. Moreover, the influence factors on predicting the rejection of the TRCs by NF membranes were analyzed. This assessment can be effective for selecting the suitable NF membrane for treating the CGB and improving the accuracy of the DSPM&DE model.

2. Materials and methods

2.1. Experimental set-up and operation protocol

For the laboratory experiment, the equipment was fitted with an 1812 spiral-wound module that provides a filtration area of 0.36 m². The crossflow filtration was adopted, and a cross-flow velocity of 0.30 m s^{-1} was considered. The permeate and concentrate of the NF membranes were collected in a 1.0 m³ tank. The NF laboratory-scale experiment was conducted with OWNF1 (Originwater, China), NF-270 (Dow/Filmtec, USA) and Desal-5 DK (GE Osmonics, USA). These NF membranes use different materials. The OWNF1 and Desal-5 DK use polyamide, while NF270 is a semi-aromatic piperazine-based polyamide. The MWCO of OWNF1, Desal-5 DK and NF270 are 200–400, 270–300 and 150–300 Da, respectively [6].

New membranes were immersed in deionized water for 24 h, and then flushed with deionized water for 1.0 h in 2.0 bar to eliminate the compression effect before the rejection experiment [19]. The filtration tests followed the same procedure. Considering the reasonable membrane flux, the pressure was set to 0.1–0.7 bar (OWNF1) and increased from 1.0 to 3.5 bar (NF270 and Desal-5 DK). 10 mg L^{-1} of glucose and 10 mmol L^{-1} of NaCl were tested to obtain the NF membrane parameters. The TRCs of the CGB and 10 mmol L^{-1} of NaCl were mixed and added to the deionized water. The concentration of each of the organic compounds was 20 mg L^{-1}. The water temperature of the practical application was approximately 20°C, and which was adopted in this experiment.

2.2. TRCs of CGB

The TRCs used for the rejection experiments were considered based on their varied physicochemical properties.

As listed in Table 1, the TRCs in the CGB comprise long chain *n*-alkanes [2], polynuclear aromatic hydrocarbons [3], esters, heterocycles, carboxylic acids, alcohols, ketones and amides [4–6]. Their MW is mostly in the range of 100 to 350 Da. The charge of the TRCs was determined based on the ChemAxon and Lange's Handbook of Chemistry, which shows that most of the TRCs are uncharged. The logP was obtained from ChemSpider (Table 2).

2.3. Analytical methods

The concentration values of the TRCs were detected using the high-performance liquid chromatography (LC-20AT, Shimadzu, Japan). The glucose concentration was determined using the iodometric method. The chloride concentration was measured using an ion chromatographic analyzer (Dionex ICS-1100, USA).

2.4. Prediction of rejection ratio using the DSPM&DE model

Membrane average pore radius (r_p), effective membrane thickness (δ), surface charge density (χ) and dielectric constant (ε) are the parameters essential for applying the DSPM&DE model to predict the rejection ratios of the organic compounds [20,21].

The values of effective membrane thickness (δ) and average pore radius (r_p) were determined by fitting the results of glucose rejection obtained from the testing in Eq. (1) [16]. The characteristics of the uncharged TRCs were not affected by other solutes. Therefore, the equation of rejection of the uncharged TRCs relies on the value of membrane average pore radius (r_p).

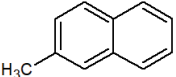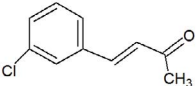$$R = 1 - \frac{K_{ic}\varphi_i}{1 - \exp\left(-\dfrac{J_V K_{ic}\delta}{D_{ip}}\right)(1 - K_{ic}\varphi_i)} \tag{1}$$
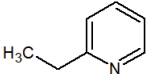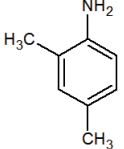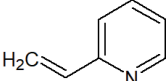
where K_{ic} is the convective hindrance factor, J_V is the total volume flux, ϕ_i is the steric partitioning coefficient, and D_{ip} is the hindered diffusivity.

The value of membrane surface charge density (χ) was calculated using the NaCl rejection test and Eq. (2) [22], which

Table 1
Properties of TRCs of the CGB

TRCs	Category	Molecular formula	MW (Da)	Stokes radius (nm)	Charge (pH 7)
Dibutyl phthalate	Ester	$C_{16}H_{22}O_4$	278.34	0.447	0
Hexanedioic acid, diisooctyl ester	Ester	$C_{22}H_{42}O_4$	370.56	0.505	0
Isopropyl stearate	Ester	$C_{21}H_{42}O_2$	326.56	0.478	0
Diisodecyl phthalate	Ester	$C_{28}H_{46}O_4$	446.66	0.547	0
3,7,11-Trimethyl-3-Dodecanol	Octanols	$C_{15}H_{32}O$	228.41	0.410	0
1-Propanol,2-(2-methoxypropoxy)-	Octanols	$C_7H_{16}O_3$	148.2	0.341	0
3-Hexanol	Octanols	$C_6H_{14}O$	102.18	0.290	0
Undecane	Alkane	$C_{11}H_{24}$	156.31	0.349	0
Dodecane	Alkane	$C_{12}H_{26}$	170.34	0.362	0
Tetradecane	Alkane	$C_{14}H_{30}$	198.39	0.386	0
8-Hexyl-8-pentyl-hexadecane	Alkane	$C_{27}H_{56}$	380.73	0.511	0
Eicosane	Alkane	$C_{20}H_{42}$	282.55	0.450	0
Tricosane	Alkane	$C_{23}H_{48}$	324.63	0.477	0
3-Chloro-benzalacetone	Ketone	$C_{10}H_9ClO$	180.63	0.371	0
Cyclohexanone,2-acetyl-	Ketone	$C_8H_{12}O_2$	140.18	0.333	0
2-Methylnaphthalene	Naphthalene	$C_{11}H_{10}$	142.20	0.335	0
1-Methylnaphthalene	Naphthalene	$C_{11}H_{10}$	142.20	0.335	0
Pentanamide	Amide	$C_5H_{11}NO$	101.15	0.289	0
Acetamide	Amide	CH_3CONH_2	59.068	0.229	0
1,2,4,5-Tetramethyl benzene	Benzene	$C_{10}H_{14}$	134.22	0.326	0
3-Cyclopentene-1-acetaldehyde, 2,2,3-trimethyl-	Aldehyde	$C_{10}H_{16}O$	152.23	0.345	0
5-(Hexadecyloxy)-2-pentadecyl-1,3-dioxane	Dioxane	$C_{35}H_70$	538.93	0.593	0
3,3,5,5-Tetramethyl cyclopentene	Cyclopentene	C_9H_{16}	124.22	0.316	0
2-Amino-4-methylpyrimidine	Pyrimidine	$C_5H_7N_3$	109.13	0.299	0
2-Ethylpyridine	Pyridine	C_7H_9N	107.156	0.296	+1
2-Vinylpyridine	Pyridine	C_7H_7N	105.14	0.294	+1
4-Isopropylpyridine	Pyridine	$C_8H_{11}N$	121.183	0.312	+1
Indole	Indole	C_8H_7N	117.14	0.308	0
2,4-Dimethylaniline	Aniline	$C_8H_{11}N$	121.183	0.312	+1

Table 2
Molecular structure of six targets TRCs of the CGB

TRCs	Molecular structure	Molecular length (A)	Molecular width (A)	logP	pKa
Undecane		12.96	0.75	6.60	
2-Methylnaphthalene		6.56	3.02	3.86	
3-Chloro-benzalacetone		9.11	4.14	2.78	
2-Ethylpyridine		5.20	3.02	1.72	5.89
2,4-Dimethylaniline		3.92	6.04	1.86	4.89(+1) (25°C)
2-Vinylpyridine		5.20	3.02	1.34.	4.98(+1) (25°C)

was based on a simplification of the general DSPM&DE model equations [22]. The prediction approach was applied in the negatively charged membrane, neutral membrane and positively charged membrane [23]. The concentrations of the TRCs were much lower than that of the sodium chloride, and the TRCs did not influence the value of surface charged density (χ). Therefore, the rejection performance of NaCl determines the value of membrane surface charged density (χ).

$$R = 1 - \frac{K'_{2eff}}{2}\left(r_0 + \frac{1-\Lambda}{G-1}\right) \times \left(\sqrt{\frac{\chi^2}{z_1^2 c_1^2\left(0^-\right) + 4\varphi_1\varphi_2 \exp\left(-2z_1^2 \Delta W_0\right)}} + \frac{\chi}{z_1 c_1\left(0^-\right)}\right) \tag{2}$$

where ΔW_0 is the excess solvation energy, K'_{2eff} is the effective convective, z_1 is the cation ionic valence, c_1 is the cation mole concentration, and 0^- is the feed side of feed/membrane interface. Λ, G and r_0 are parameters that are defined, dimensionless.

According to the three assumptions about the dielectric phenomenon of the DSPM&DE model, the dielectric constant of the membrane pore is equal to the bulk solution because the variations in the solvent properties caused by its confinement in small narrow pores are neglected, and the separation effect of polarization charges along the membrane pores is not relevant in determining the rejection of ions [24]. ΔW_0 and ΔW_δ used in Eq. (2) represent the dielectric effect at the interface of the feed/membrane and membrane/permeate, respectively. These are the energy terms related to the dielectric constant as defined in the following equations:

$$\Delta W_0 = r_B\left\{\kappa\left(0^-\right) - \kappa\left(0^+\right) - \frac{1}{r_p}\ln\left[1 - \gamma\exp\left(-2r_p\kappa\left(0^+\right)\right)\right]\right\} \tag{3a}$$

$$\Delta W_\delta = r_B\left\{\kappa\left(\delta^-\right) - \kappa\left(\delta^+\right) - \frac{1}{r_p}\ln\left[1 - \gamma\exp\left(-2r_p\kappa\left(\delta^+\right)\right)\right]\right\} \tag{3b}$$

The equations related to the calculation of the parameters in the above equations are summarized in Table S1.

3. Results and discussion

3.1. Performance of rejecting uncharged TRCs

The membrane flux increases with steadily increasing operation pressure, as known well. An upward trend of the NF membrane flux is observed in the separation experiment (Fig. 1). The NF membranes flux appear controlled in the range of 6.21 to 42.73 L m^{-2} h^{-1}.

The separation performance of undecane was used to illustrate the rejection mechanism of uncharged TRCs and/or the long-chain *n*-alkanes in the CGB. As shown in Fig. 2, the undecane rejection ratio of NF270 is 95.26% at 11.42 L m^{-2} h^{-1}, which then gradually increases to 98.52% at 42.04 L m^{-2} h^{-1}. The relatively high rejection ratio indicated that undecane could be effectively rejected by the steric hindrance effect of the intrinsic porosity of NF membrane, although the MW (156.31 Da) of undecane was below the MWCO of NF membranes. Moreover, Fig. 2 also shows that the undecane rejection ratio of OWNF1, which increases from 65.49% (12.34 L m^{-2} h^{-1}) to 87.73% (42.73 L m^{-2} h^{-1}), is lower than that of NF270 (29.77% and 10.79%).
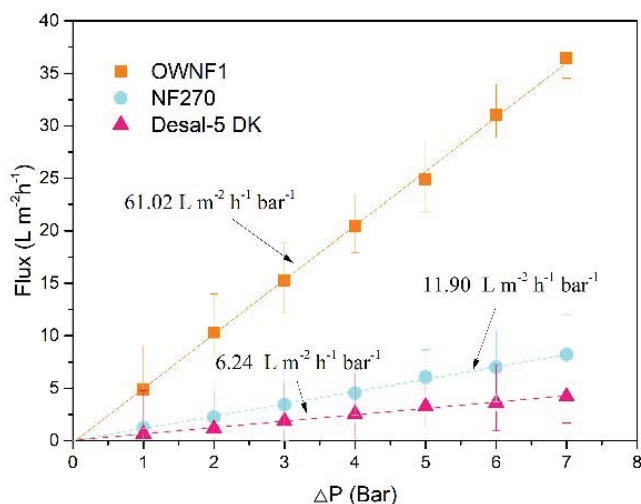
Fig. 1. Total volume flux as a function of the effective pressure difference across membranes. The experimental temperature is 20°C.
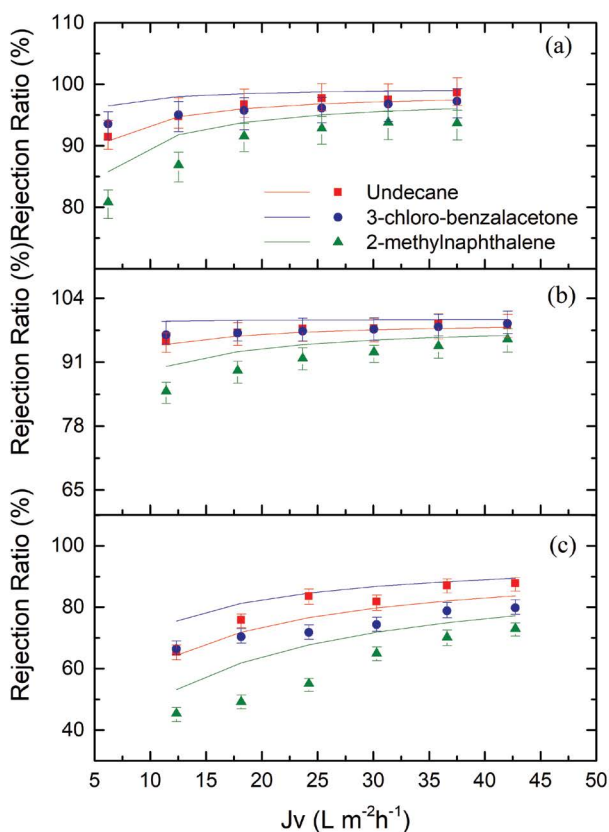

Fig. 2. Rejection ratios of the uncharged TRCs in the CGB by NF membranes. The symbols are experimental values and the curved lines are predicted rejection ratios using the DSPM&DE model. (a) Desal-5 DK, (b) NF270 and (c) OWNF1.

The separation experiment of 3-chloro-benzalacetone conducted using the NF membranes was investigated to compare the rejection performance of the uncharged TRCs with low MW. The undecane of NF270 demonstrates a rejection ratio marginally higher than that of 3-chloro-benzalacetone. Particularly, the rejection ratio of 3-chloro-benzalacetone by NF270 gradually increases from 96.35% at 1.24 L m^{-2} h^{-1} to 98.66% at 6.98 L m^{-2} h^{-1} (Fig. 2). Among the three NF membranes, the highest rejection of undecane is obtained by NF270. This phenomenon could be explained by the fact that the removal efficiency of the uncharged TRCs closely corresponded to the relative ratio of size of the TRCs to the membrane pore radius [25]. However, two other NF membranes exhibit different rejection performances with a lower rejection ratio of 3-chloro-benzalacetone in contrast to undecane. The molecular lengths of 3-chloro-benzalacetone and undecane are 9.11 and 12.96 A, respectively, as listed in Table 1. Therefore, it could be assumed that it was easier for 3-chloro-benzalacetone to pass through membrane with the same pore radius. This phenomenon indicated that the molecular length was more significant than the width for organic compounds rejection, as observed by Chen et al. [15] and Kiso et al. [26]. However, this phenomenon was not observed in the smaller membrane pore, because the effect of molecular width on rejection was enhanced.

According to the experimental results, the order of the rejection ratio of three NF membranes is shown as follows (Fig. 2): OWNF1 < Desal-5 DK < NF270. The rank indicated that the rejection ratio of the TRCs was closely associated with the pore sizes of nanofiltration membrane and the molecular structure of TRCs. The rejection performance of the uncharged TRCs could be effectively improved using the NF membrane with a small membrane pore radius.

3.2. Rejection performance of the positively charged TRCs

Fig. 3 illustrates the rejection performance of the three positively charged TRCs, including 2-vinylpyridine, 2-ethylpyridine and 2,4-dimethylaniline. The electrostatic attraction could be generated between the positively charged TRCs and negatively charged membrane [27]. Further, the positively charged TRCs could be accumulated on the negatively charged membrane and diffuse through it more easily [28]. The experimental results indicate that the rejection ratio of 2-vinylpyridine of OWMF1 is 24.4% under the flux of 12.34 L m^{-2} h^{-1}, which then gradually increases to 49.68% at 42.73 L m^{-2} h^{-1}. Generally, a higher membrane charge density decreases the rejection of positively charged TRCs because of the elimination of dielectric exclusion due to the suppression of the fixed charges and predominant role of Donnan effect during the NF process [29]. Nevertheless, the rejection of 2-vinylpyridine of NF270 and the Desal-5 DK are observed to be approximately 82.66% and 78.59%, respectively. In contrast to the rejection of Desal-5 DK, a higher rejection of 2-vinylpyridine is obviously observed in the experiment of NF270, which demonstrates a higher membrane charge density and a smaller membrane pore radius. Hence, it could be speculated that the rejection performance of positively charged TRCs was determined by both the electrostatic attraction effect and steric hindrance effect, while the steric hindrance effect plays the primarily role.

3.3. Prediction of the TRCs rejection ratio using DSPM&DE model

The rejection function of DSPM&DE model is related to the membrane parameters that include the membrane
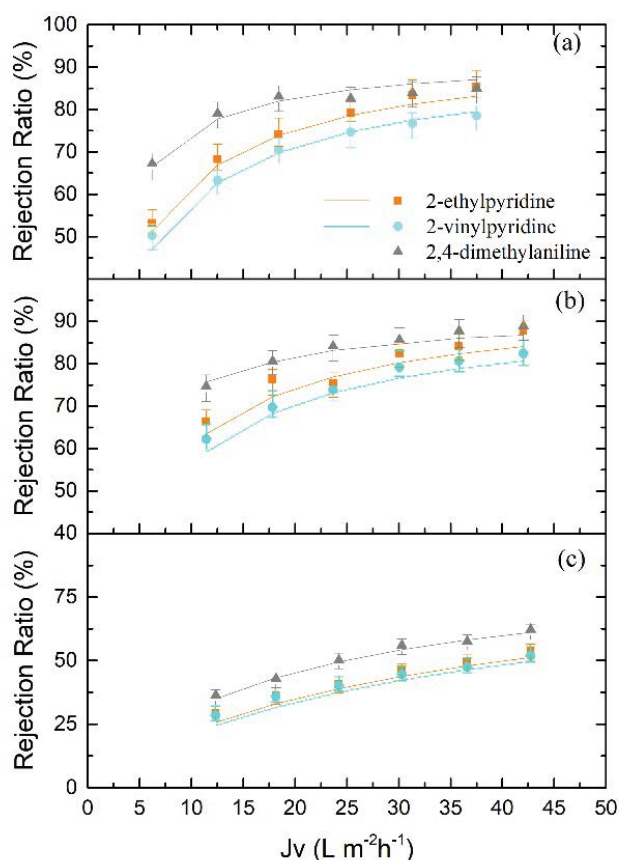
Fig. 3. Rejection ratios of the positively charged TRCs in the CGB by NF membranes. (a) Desal-5 DK, (b) NF270 and (c) OWNF1.

pore radius, surface charge density, and effective membrane thickness and dielectric constant [22,24]. The surface charge density was introduced in the extended Nernst–Planck equation by Kotrappanavar et al. [16] and Tsuru et al. [30] to analyze the experimental results of separating monovalent ions and divalent ions using the negatively charged reverse osmosis membranes. The surface charge density is accounted for the fixed charge located in the whole membrane volume referring to a homogeneous distribution and provided as a function of equivalent concentration existing at the feed/membrane interface. The calculation of the surface charge density is associated with the rejection of sodium chloride, and the model calculation procedure detailed elucidated elsewhere [25]. The experimental results indicated that the membrane pore radius of OWNF1, NF270 and Desal-5 DK was 0.52, 0.40 and 0.42 nm and their membrane thickness was 2.10, 0.75 and 1.60 μm, respectively. The values of charge density of three NF membranes indicated that the NF membranes used for testing were all negatively charged.

The rejection ratio of undecane, representing the uncharged TRCs in the CGB, was predicted by substituting the values of the parameters, including the membrane pore radius, the effective membrane thickness and the undecane radius in Eq. (1). The undecane rejection of NF270 demonstrated an upward tendency and improved by 3.44%, when the membrane flux steadily increased from 11.42 to 42.04 L m⁻² h⁻¹.

It is noteworthy that the DSPM&DE model predicted an undecane rejection lower than that obtained by the experiment. The deviation between the predicted rejection and experimental value was considered to be related to the Stokes radius, which was based on the assumption of DSPM&DE model that the molecules were spherical in shape and rigid [31]. Therefore, the parameter may not exactly represent the long-chain structure of undecane. Furthermore, the molecular width, molecular length and the log$P$ value are important factors in predicting the rejection ratio of the uncharged TRCs. It can be concluded from the experimental results that predicting the rejection of uncharged TRCs was not just based on the molecular width or molecular length. Agenson et al. [32] also observed this phenomenon in the experiment of removing organics from wastewater by the NF membranes. The prediction rejection of the model was also conducted for the other two uncharged TRCs that included 2-methylnaphthalene and 3-chloro-benzalacetone. The prediction results of the DSPM&DE model agreed accurately with the experimental values obtained.

The rejection of 2,4-dimethylaniline with positively charge was predicted by the DSPM&DE model. The predicted rejection of 2,4-dimethylaniline of NF270 was 84.63% (30.06 L m⁻² h⁻¹) which was 1.04% less than compared with the experimental rejection. The rejection ratios of the other two positively charged TRCs in CGB, including 2-vinylpyridine and 2-ethylpyridine, were lower-predicted approximately 2.52% and 2.09%. This indicates that the DSPM&DE model demonstrated a marginal deviation from the experiment in predicting the rejection ratios of positively charged TRCs in the CGB. This conclusion was also discussed by Wang et al. [33] in their study, in which they applied the DSPM&DE model to predict the rejection of the positively charged organics. Verliefde et al. [34] reported that the predicted rejection being lower could be explained by the difference between the membrane potential of the model and real membrane potential. However, the explanation for the predicted rejection
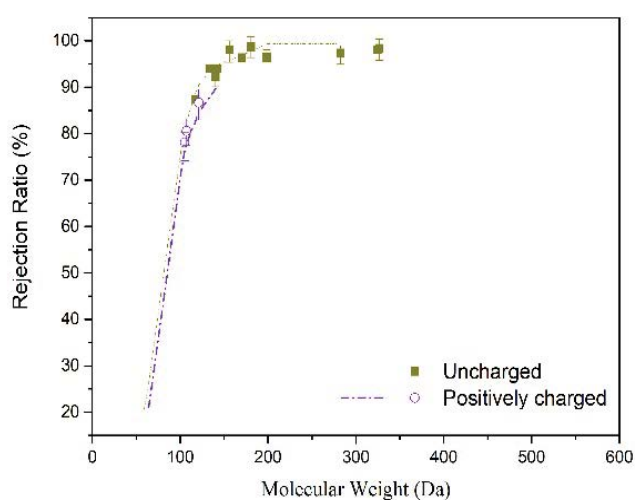

Fig. 4. Rejection ratio of the 14 TRCs by NF270. The TRCs is divide into two groups: the uncharged TRCs and positively charged TRCs. The symbols represent the experimental results and the curved lines are predicted rejection by fitting DSPM&DE model.
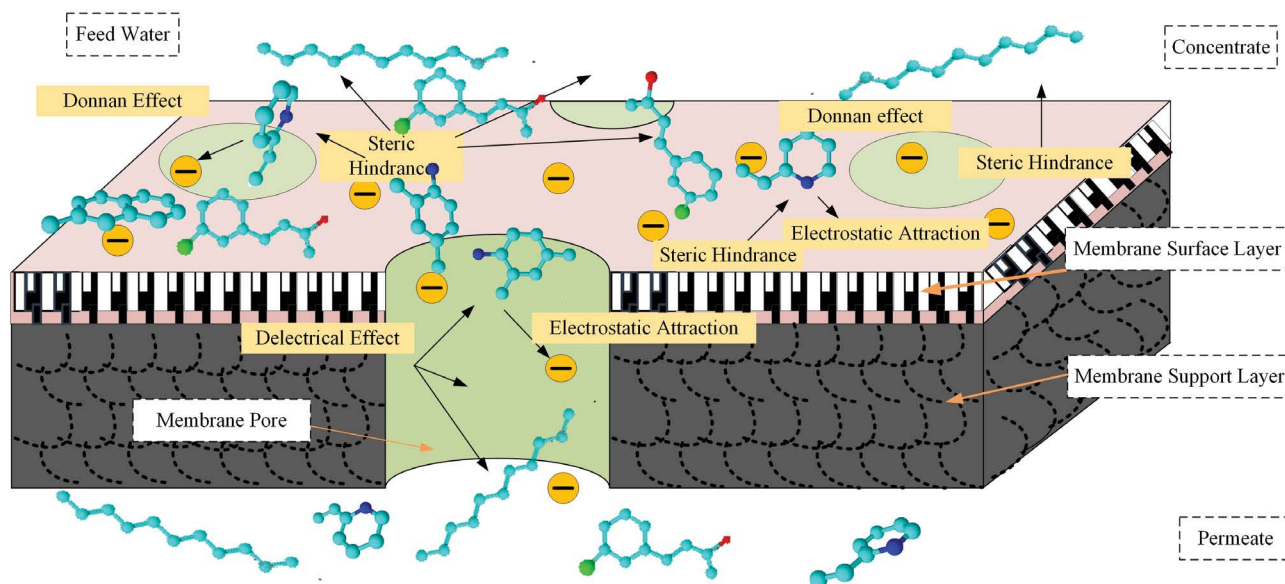
Fig. 5. Conceptual sketch of rejection mechanism of the TRCs with different charge and low MW by NF membranes.

of positively charged organics being lower is not definitive and adequate.

It was recognized that the separation mechanism is remarkably related to the steric and electrostatic partitioning effects between the membrane and external solutions [22]. These positively charged TRCs were most probably in the incomplete dissociated form, and therefore the Donnan effect in the interface of feed/membrane and membrane/permeate, as the electrostatic partitioning effects, is weaker in this experiment than that in the modeling process. In addition, the DSPM&DE model simplified the hydrophobic parameter [20], and the hydrophobic parameter of 2,4-dimethylaniline (log$P$ = 1.86) and 2-vinylpyridine (log$P$ = 1.72) would be similar. Hence, it could not be inferred from the result whether hydrophobicity was an influence factor that caused an underestimation of the predicted rejection.

The rejection performance of 14 TRCs by NF270 in this experiment and the model prediction, including 11 uncharged TRCs and 3 positively charged TRCs, is presented for comparison (Fig. 4). These results confirm that the DSPM&DE model generally accurately predicts the rejection ratios of the TRCs. Meanwhile, the predicted rejection shows a steeply ascendant trend and steadily attains an asymptotical state, when the MW of TRCs increases. Fig. 4 further illustrates that the positively charged TRCs demonstrate a poorer rejection ratio compared with the uncharged TRCs with a similar MW. As mentioned in Section 3.2, the lower rejection of the positively charged TRCs may be caused by the accumulation on the negatively charged membrane and rendered these TRCs more readily pass through the NF membrane. Moreover, the simplification calculation of the Donnan potential in terms of the dielectric constant and the dissolution was possibly the cause of lower predicted rejection of the positively charged TRCs. In this case, these positively charged TRCs were weakly charged so that the dielectric exclusion and the Donnan effect did not significantly affect the rejection ratio compared with the steric hindrance effect.

Comprehensively, the rejection ratios of the charged TRCs were determined by the steric hindrance effect, dielectric exclusion effect and Donnan effect, while the steric hindrance effect plays a primary role (Fig. 5).

4. Conclusion

The DSPM&DE model was applicable in predicting the rejection of TRCs with a low MW by NF membranes. The rejection ratios of the TRCs increased and attained the asymptotic values, when the flux ranged from 6.21 to 42.73 L m^{-2} h^{-1}. At the flux of 30.06 L m^{-2} h^{-1}, the rejection ratios of the six TRCs of NF270 have attained over 79.15%. The TRCs were divided into two groups according to the sign of the charge. The rejection ratios of the uncharged TRCs were inversely proportional to the ratio of membrane pore radius to molecular size. The steric hindrance effect was identified as the rejection mechanism that determined the mass transport of uncharged TRCs through the NF membranes. The positively charged TRCs, including the 2,4-dimethylaniline, 2-vinylpyridine and 2-ethylpyridine, displayed lower rejection ratio compared with the uncharged TRCs with similar MW because the electrostatic attraction between these positively charged TRCs and negatively charged membrane surface facilitated the transportation of TRCs through the NF membrane. The marginal discrepancy of the experimental rejection and predicted rejection by the DSPM&DE model could be explained by the interaction of solute–membrane, mass transfer and the TRCs partition to the membrane material. Generally, the DSPM&DE model is applicable for predicting the rejection of the TRCs by revising the TRCs partition in the solute–membrane and membrane pore.

Acknowledgments

Symbols

c — Mole concentration, mol m^{-3}
D_{ip} — Hindered diffusivity, m^2 s^{-1}
J_V — Total volume flux, mol s^{-1}
K'_{2eff} — Effective convective coefficient, dimensionless
K_{ic} — Convective hindrance factor, dimensionless
r_p — Average pore radius, m
R — Solute rejection, dimensionless
z — Ionic valence, dimensionless
χ — Volumetric charge density, mol m^{-3}
δ — Effective membrane thickness
Φ_i — Steric partitioning coefficient, dimensionless
ΔW_0 — Excess solvation energy
$\Delta\psi_D$ — Donnan potential
ε — Dielectric constant, C^2 J^{-1} m^{-1}
κ^{-1} — Debye length, m
0^- — Feed side of the feed/membrane interface
0^+ — Membrane side of the feed/membrane interface

References

[1] H.F. Zhuang, H.J. Han, S.Y. Jia, Q. Zhao, B.L. Hou, Advanced treatment of biologically pretreated coal gasification wastewater using a novel anoxic moving bed biofilm reactor (ANMBBR)-biological aerated filter (BAF) system, Bioresour. Technol., 157 (2014) 223–230.

[2] H. Zhu, Y. Han, C. Xu, H. Han, W. Ma, Overview of the state of the art of processes and technical bottlenecks for coal gasification wastewater treatment, Sci. Total Environ., 637–638 (2018) 1108–1126.

[3] P. Xu, H. Han, H. Zhuang, B. Hou, S. Jia, D. Wang, K. Li, Q. Zhao, Anoxic degradation of nitrogenous heterocyclic compounds by activated sludge and their active sites, J. Environ. Sci.-China, 31 (2015) 221–225.

[4] F. Fang, H. Han, Q. Zhao, C. Xu, L. Zhang, Bioaugmentation of biological contact oxidation reactor (BCOR) with phenol-degrading bacteria for coal gasification wastewater (CGW) treatment, Bioresour. Technol., 150 (2013) 314–320.

[5] P. Xu, H. Han, B. Hou, H. Zhuang, S. Jia, D. Wang, K. Li, Q. Zhao, The feasibility of using combined TiO$_2$ photocatalysis oxidation and MBBR process for advanced treatment of biologically pretreated coal gasification wastewater, Bioresour. Technol., 189 (2015) 417–420.

[6] K. Li, W. Ma, H. Han, C. Xu, Y. Han, D. Wang, W. Ma, H. Zhu, Selective recovery of salt from coal gasification brine by nanofiltration membranes, J. Environ. Manage., 223 (2018) 306–313.

[7] F. Fang, H. Han, Effect of catalytic ozonation coupling with activated carbon adsorption on organic compounds removal treating RO concentrate from coal gasification wastewater, Ozone Sci. Eng., 40 (2018) 275–283.

[8] S. Jia, H. Zhuang, H. Han, F. Wang, Application of industrial ecology in water utilization of coal chemical industry: a case study in Erdos, China, J. Cleaner Prod., 135 (2016) 20–29.

[9] S. Jia, H. Han, H. Zhuang, P. Xu, B. Hou, Advanced treatment of biologically pretreated coal gasification wastewater by a novel integration of catalytic ultrasound oxidation and membrane bioreactor, Bioresour. Technol., 189 (2015) 426–429.

[10] M. Sadrzadeh, J. Hajinasiri, S. Bhattacharjee, D. Pernitsky, Nanofiltration of oil sands boiler feed water: effect of pH on water flux and organic and dissolved solid rejection, Sep. Purif. Technol., 141 (2015) 339–353.

[11] A.I. Schäfer, A. Pihlajamäki, A.G. Fane, T.D. Waite, M. Nyström, Natural organic matter removal by nanofiltration: effects of solution chemistry on retention of low molar mass acids versus bulk organic matter, J. Membr. Sci., 242 (2004) 73–85.

[12] L. Ji, Y. Zhang, E. Liu, Y. Zhang, C. Xiao, Separation behavior of NF membrane for dye/salt mixtures, Desal. Wat. Treat., 51 (2013) 3721–3727.

[13] M. Elimelech, W.H. Chen, J.J. Waypa, Measuring the zeta (electrokinetic) potential of reverse osmosis membranes by a streaming potential analyzer, Desalination, 95 (1994) 269–286.

[14] A.W. Mohammad, Y.H. Teow, W.L. Ang, Y.T. Chung, D.L. Oatley-Radcliffe, N. Hilal, Nanofiltration membranes review: recent advances and future prospects, Desalination, 356 (2015) 226–254.

[15] S.-S. Chen, J.S. Taylor, L.A. Mulford, C.D. Norris, Influences of molecular weight, molecular size, flux, and recovery for aromatic pesticide removal by nanofiltration membranes, Desalination, 160 (2004) 103–111.

[16] N.S. Kotrappanavar, A.A. Hussain, M.E.E. Abashar, I.S. Al-Mutaz, T.M. Aminabhavi, M.N. Nadagouda, Prediction of physical properties of nanofiltration membranes for neutral and charged solutes, Desalination, 280 (2011) 174–182.

[17] A. De Munari, A.J.C. Semiao, B. Antizar-Ladislao, Retention of pesticide Endosulfan by nanofiltration: influence of organic matter–pesticide complexation and solute–membrane interactions, Water Res., 47 (2013) 3484–3496.

[18] F. Kong, H. Yang, X. Wang, Y.F. Xie, Assessment of the hindered transport model in predicting the rejection of trace organic compounds by nanofiltration, J. Membr. Sci., 498 (2016) 57–66.

[19] D.L. Oatley-Radcliffe, S.R. Williams, M.S. Barrow, P.M. Williams, Critical appraisal of current nanofiltration modelling strategies for seawater desalination and further insights on dielectric exclusion, Desalination, 343 (2014) 154–161.

[20] I.I. Ryzhkov, A.V. Minakov, Theoretical study of electrolyte transport in nanofiltration membranes with constant surface potential/charge density, J. Membr. Sci., 520 (2016) 515–528.

[21] J. Schaep, C. Vandecasteele, A.W. Mohammad, W.R. Bowen, Analysis of the salt retention of nanofiltration membranes using the Donnan–steric partitioning pore model, Sep. Sci. Technol., 34 (1999) 3009–3030.

[22] S. Bandini, D. Vezzani, Nanofiltration modeling: the role of dielectric exclusion in membrane characterization, Chem. Eng. Sci., 58 (2003) 3303–3326.

[23] S. Bandini, C. Gostoli, A Simplifed Approach for Characterization and Prediction of Nanofltration Membranes Performances, Proceedings of Euromembrane Leuwen, Belgium, 1999.

[24] J.E. Almazán, E.M. Romero-Dondiz, V.B. Rajal, E.F. Castro-Vidaurre, Nanofiltration of glucose: analysis of parameters and membrane characterization, Chem. Eng. Res. Des., 94 (2015) 485–493.

[25] F. Fadaei, V. Hoshyargar, S. Shirazian, S.N. Ashrafizadeh, Mass transfer simulation of ion separation by nanofiltration considering electrical and dielectrical effects, Desalination, 284 (2012) 316–323.

[26] Y. Kiso, K. Muroshige, T. Oguchi, T. Yamada, M. Hhirose, T. Ohara, T. Shintani, Effect of molecular shape on rejection of uncharged organic compounds by nanofiltration membranes and on calculated pore radii, J. Membr. Sci., 358 (2010) 101–113.

[27] S. Bandini, Modelling the mechanism of charge formation in NF membranes: theory and application, J. Membr. Sci., 264 (2005) 75–86.

[28] A.D. Shah, C.-H. Huang, J.-H. Kim, Mechanisms of antibiotic removal by nanofiltration membranes: model development and application, J. Membr. Sci., 389 (2012) 234–244.

[29] A. Szymczyk, P. Fievet, Investigating transport properties of nanofiltration membranes by means of a steric, electric and dielectric exclusion model, J. Membr. Sci., 252 (2005) 77–88.

[30] T. Tsuru, M. Urairi, S. Nakao, S. Kimura, Reverse osmosis of single and mixed electrolytes with charged membranes: experiment and analysis, J. Chem. Eng. Jpn., 24 (1991) 518–524.

[31] C. Bellona, J.E. Drewes, P. Xu, G. Amy, Factors affecting the rejection of organic solutes during NF/RO treatment: a literature review, Water Res., 38 (2004) 2795–2809.

[32] K.O. Agenson, J.-I. Oh, T. Urase, Retention of a wide variety of organic pollutants by different nanofiltration/reverse osmosis membranes: controlling parameters of process, J. Membr. Sci., 225 (2003) 91–103.

[33] X. Wang, B. Li, T. Zhang, X. Li, Performance of nanofiltration membrane in rejecting trace organic compounds: experiment and model prediction, Desalination, 370 (2015) 7–16.

[34] A.R.D. Verliefde, E.R. Cornelissen, S.G.J. Heijman, J. Verberk, G.L. Amy, B. Van der Bruggen, J.C. van Dijk, The role of electrostatic interactions on the rejection of organic solutes in aqueous solutions with nanofiltration, J. Membr. Sci., 322 (2008) 52–66.

Supplementary information

Table S1
Calculation equation of DSPM&DE model [22]

Concentration and potential gradients through the membrane:

$$\frac{dc_i}{dx} = \frac{J_V}{D_{ip}}\Big[K_{ic}c_i - c_i\big(\delta^+\big)\Big] - \frac{z_i c_i F}{RT}\frac{d\psi}{dx}$$

$$\frac{d\psi}{dx} = \frac{\sum_{i=1}^{n} z_i \frac{J_V}{D_{ip}}\Big[K_{ic}c_i - c_i\big(\delta^+\big)\Big]}{\left(\frac{F}{RT}\right)\sum_{i=1}^{n} z_i^2 c_i}$$

Partitioning equations at membrane/external solutions interfaces:

$$\frac{c_i\big(0^+\big)}{c_i\big(0^-\big)} = \phi_i \exp\big(-z_i \Delta\psi_{D0}\big)\exp\big(-z_i^2 \Delta W_0\big)$$

$$\frac{c_i\big(\delta^+\big)}{c_i\big(\delta^-\big)} = \phi_i \exp\big(-z_i \Delta\psi_{D\delta}\big)\exp\big(-z_i^2 \Delta W_\delta\big)$$

Electroneutrality conditions:

$$\sum_{i=1}^{n} z_i\, c_i\big(\delta^+\big) = 0$$

$$\sum_{i=1}^{n} z_i\, c_i - \chi = 0$$

Membrane charge density:

$$\chi = q c_{eqv}^s \qquad c_{eqv} = \frac{1}{2}\sum_{i=1}^{n}\big|z_i\big| c_i\big(0^-\big)$$

In which

$$J_i = J_V c_i\big(\delta^+\big)$$

$$D_{ip} = K_{id} D_{i\infty}$$

Steric partitioning:

$$\phi_i = \big(1-\lambda_i\big)^z, \quad \lambda_i = \frac{r_i}{r_p}$$

Hindrance factors:

$$0 < \lambda_i \leq 0.8$$

$$K_{ic} = 1.0 + 0.054\lambda_i - 0.988\lambda_i^2 + 0.441\lambda_i^3$$

$$K_{id} = 1.0 - 2.30\lambda_i + 1.154\lambda_i^2 + 0.224\lambda_i^3$$

$$0.8 < \lambda_i \leq 1$$

$$K_{ic} = -6.830 + 19.348\lambda_i - 12.518\lambda_i^2$$

$$K_{id} = -0.105 + 0.318\lambda_i - 0.213\lambda_i^2$$

Defined parameter used in equations:

$$r_B = \frac{F^2}{8\pi\varepsilon_p RTN_A}$$

$$\gamma = \frac{1-\varepsilon_M/\varepsilon_P}{1+\varepsilon_M/\varepsilon_P}$$

$$\kappa^{-1}\big(0^-\big) = \frac{1}{F}\sqrt{\frac{\varepsilon PRT}{2I\big(0^-\big)}}$$

$$\kappa^{-1}\big(0^+\big) = \frac{1}{F}\sqrt{\frac{\varepsilon_p RT}{2I\big(0^-\big)}}$$

$$I\big(0^-\big) = \frac{1}{2}\sum_{i=1}^{n} z_i^2 c_i\big(0^-\big)$$